Identification of Key Amino Acid Residues in the Assembly of Enzymes into the Pyruvate Dehydrogenase Complex of *Bacillus stearothermophilus*: A Kinetic and Thermodynamic Analysis[†]

Hyo-Il Jung,[§] Alan Cooper,[‡] and Richard N. Perham*,[§]

Cambridge Centre for Molecular Recognition, Department of Biochemistry, University of Cambridge, 80 Tennis Court Road, Cambridge CB2 1GA, United Kingdom, and Department of Chemistry, University of Glasgow, Glasgow G12 8QQ, United Kingdom

ABSTRACT: Structural studies have shown that electrostatic interactions play a major part in the binding of dihydrolipoyl dehydrogenase (E3) to the peripheral subunit-binding domain (PSBD) of the dihydrolipoyl acyltransferase (E2) in the assembly of the pyruvate dehydrogenase multienzyme complex of *Bacillus stearothermophilus*. The binding is characterized by a small, unfavorable enthalpy change ($\Delta H° = +2.2$ kcal/mol) and a large, positive entropy change ($T\Delta S° = +14.8$ kcal/mol). The contributions of individual surface residues of the PSBD of E2 to its interaction with E3 have been assessed by alanine-scanning mutagenesis, surface plasmon resonance detection, and isothermal titration calorimetry. The mutation R135A in the PSBD gave rise to a significant decrease (120-fold) in the binding affinity; two other mutations (R139A and R156A) were associated with smaller effects. The binding of the R135A mutant to E3 was accompanied by a favorable enthalpy ($\Delta H° = -2.6$ kcal/mol) and a less positive entropy change ($T\Delta S° = +7.2$ kcal/mol). The midpoint melting temperature (T_m) of E3-PSBD complexes was determined by differential scanning calorimetry. The R135A mutation caused a significant decrease (5 °C) in the T_m, compared with the wild-type complex. The results reveal the importance of Arg135 of the PSBD as a key residue in the molecular recognition of E3 by E2, and as a major participant in the overall entropy-driven binding process. Further, the effects of mutagenesis on the ΔC_p of subunit association illustrate the difficulties in attributing changes in heat capacity to specific classes of interactions.

The oxidative decarboxylation of pyruvate is carried out by the successive action of three enzymes of the pyruvate dehydrogenase (PDH)[1] complex: pyruvate decarboxylase (E1, E.C. 1.2.4.1), dihydrolipoyl acetyltransferase (E2, E.C. 2.3.1.12), and dihydrolipoyl dehydrogenase (E3, E.C. 1.8.1.4). E1 catalyzes both the decarboxylation of pyruvate and the subsequent reductive acetylation of a lipoyl group covalently bound to the E2; E2 catalyzes the transfer of the acetyl group to CoA; and E3 catalyzes the reoxidation of the resultant dihydrolipoyl moiety, with NAD^+ as the ultimate electron acceptor (*1−4*).

The PDH complex of *Bacillus stearothermophilus* is typical and one of the best studied. Its icosahedral E2 core is made up of 60 E2 chains. Each E2 chain has a multidomain-and-linker structure composed of three major separate folding units: an N-terminal lipoyl domain (LD, ~80 residues), a peripheral subunit-binding domain (PSBD, ~35 residues), and a C-terminal catalytic (acetyltransferase) domain (CD, ~250 residues), connected by long and highly flexible linker regions (~25−40 residues) rich in proline, alanine, and charged amino acids (*4, 5*). The acetyltransferase domain aggregates to form trimers, 20 of which are assembled to generate the inner core of the PDH complex (*6*).

The PSBD, located between the LD and CD domains, is the smallest known globular protein domain that lacks a stabilizing disulfide bridge or metal ion. The three-dimensional solution (*7*) and crystal (*8*) structures of the PSBD show it to have a compact structure stabilized mainly by hydrophobic interactions, consisting of two short and almost parallel α-helices (H1 and H2), a turn of 3_{10}-helix, and loops (L1 and L2) joining these structural elements. The main function of the PSBD is to attach both E1 and E3 to the E2 core (*9−11*). The stoichiometry and kinetics of the interactions have been closely investigated by means of nondenaturing polyacrylamide gel electrophoresis and surface plasmon resonance (SPR) analysis (*11, 12*). One *B. stearo-*

* Corresponding author.
[§] University of Cambridge.
[‡] University of Glasgow.

[1] Abbreviations: PDH, pyruvate dehydrogenase; E1, pyruvate decarboxylase (EC 1.2.4.1); E2, dihydrolipoyl acetyltransferase (EC 2.3.1.12); E3, dihydrolipoyl dehydrogenase (EC 1.8.1.4); PSBD, peripheral subunit-binding domain; LD, lipoyl domain; CD, catalytic domain; DD, di-domain; SPR, surface plasmon resonance; ITC, isothermal titration microcalorimetry; DSC, differential scanning calorimetry; HBS, Hepes buffered saline.
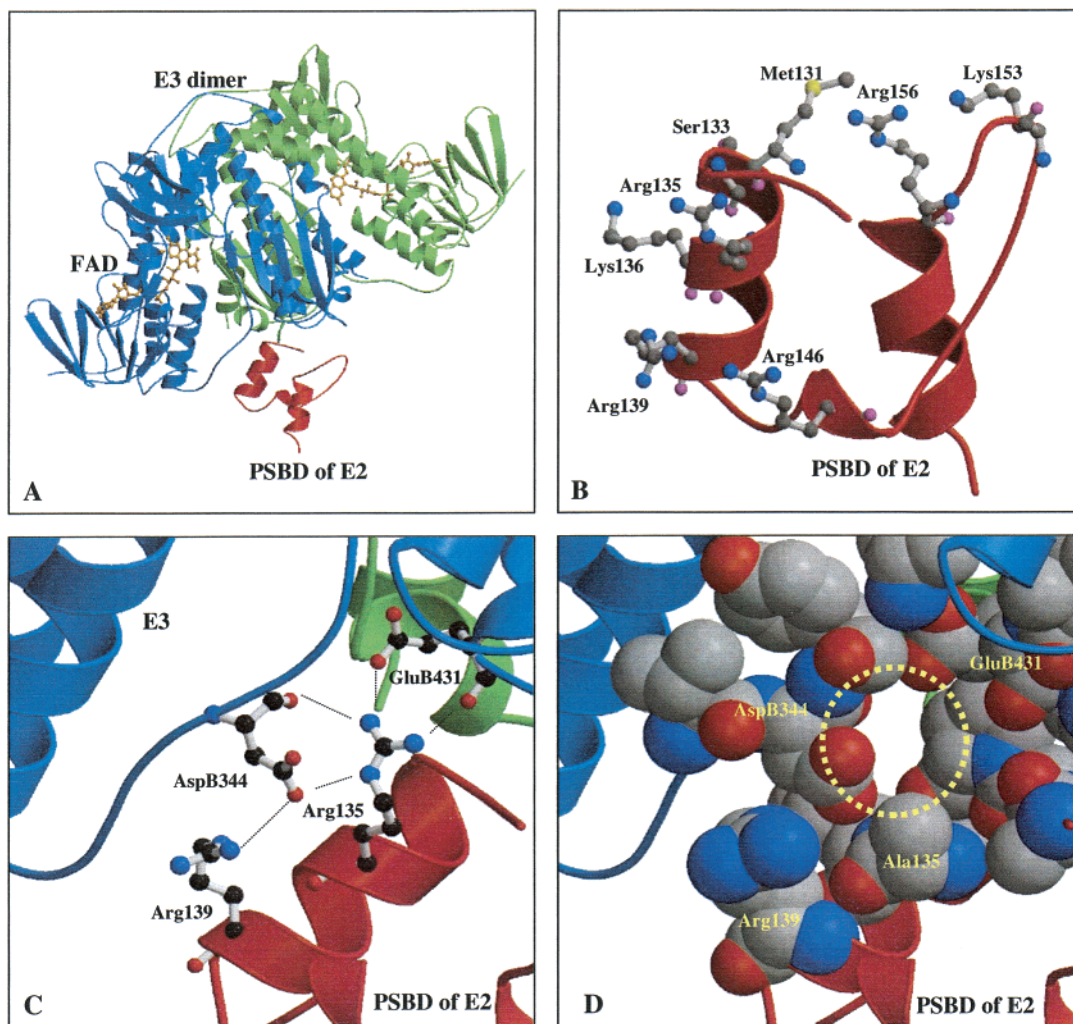
FIGURE 1: (A) Crystal structure of E3 complexed with the PSBD of E2 from *B. stearothermophilus* (*8*). The two monomers of E3 are shown in blue and green and the PSBD in red. This figure was drawn with MOLSCRIPT (*39*). (B) Surface residues of PSBD selected for alanine-scanning mutagenesis. (C) Details of the electrostatic zipper formed between acidic residues (Asp344, Glu431) of E3 and basic residues (Arg135, Arg139) of wild-type PSBD. (D) The R135A mutant was modeled with a SWISS-MODEL program (*22*). The cavity created by the R135A mutation is indicated by a yellow circle. The orientation in all four panels is the same.

thermophilus PSBD (i.e., in effect one E2 chain) is capable of binding tightly either one E1 ($\alpha_2\beta_2$) heterotetramer or one E3 dimer, but not both simultaneously. The dissociation constant (K_d) for the complex formed with E3 (5.8×10^{-10} M) was found to be almost 2-fold higher than that for the complex with E1 (3.2×10^{-10} M). The binding causes no major conformational change (*8*) and is without effect on the catalytic activity of either E1 or E3 (*11*).

The crystal structure of the *B. stearothermophilus* E3 complexed with the PSBD of the E2 chain has been solved to 2.6 Å resolution (*8*) (Figure 1A). A single E3 dimer is capable of binding only one PSBD because of steric hindrance between two PSBDs across the 2-fold axis, as surmised from earlier biochemical studies (*10*, *11*). The crystal structure also indicated that residues Arg135, Arg139, and Arg156 of the PSBD (the numbering is that of the intact E2 chain) are involved in an "electrostatic zipper" with residues Asp344 and Glu431 from one subunit of the E3 dimer, and that residues Ser133 and Lys136 make interactions with the other subunit of E3 (*8*). Thus, electrostatic interactions were proposed as the dominant driving force for the assembly of the E3-PSBD complex, but the specific roles of individual residues could not be deduced. For this, a real-

time study of the interaction in solution is required. SPR detection has previously been used to establish the kinetic constants for the interaction of wild-type PSBD with E1 and E3 (*12*). Likewise, microcalorimetry has revealed that the binding of E3 to the wild-type PSBD at 25 °C, pH 7.4, is governed by a small unfavorable enthalpy change ($\Delta H° = +2.2$ kcal/mol) and a large positive entropy change ($T\Delta S° = +14.6$ kcal/mol). It appears likely that this can be attributed to the release of water molecules accompanying the formation of salt bridges at the binding interface, greatly overcoming thereby the loss of configurational entropy (*13*).

In this paper, we describe the use of SPR and microcalorimetry to study the interaction of a series of mutant PSBDs with E3. This has led us to identify a key residue on the PSBD that dominates the electrostatic attractions, throwing new light on the overall entropy-driven binding process that underlies E3−E2 interaction. These studies also have interesting general implications for our understanding of the noncovalent forces involved in protein−protein interactions.

MATERIALS AND METHODS

Materials. All reagents used were of analytical grade unless otherwise stated. Plasmid pET11ThDD, encoding

residues 1−170 of the *B. stearothermophilus* E2p chain with a thrombin-cleavage site in the linker region between the LD and PSBD, has been described elsewhere (*14*). *Escherichia coli* lipoate protein ligase (*15*) was a gift of Mr. C. Fuller.

Design of Oligonucleotides. The following mutagenic oligonucleotides, designed to replace the indicated wild-type amino acid residues with alanine, were used:

5′-end primer: 5′-GATAACAATTCCCCTCTAGAAA-3′

3′-end primer: 5′-GCGGGATATCCGGATATAGT-3′
M131A: 5′-CGCCGCGTCATCGCCGCTCCATCCGTG-3′ (forward)

5′-GCGCACGGATGGAGCGGCGATGAC-3′ (reverse)
S133A:5′-CATGCCGGCCGTGCGCAAGT-3′

5′-ATACTTGCGCACGGCCGGCATGGCGAT-3′
R135A: 5′-ATGCCGTCCGTGGCAAAGTATGC-3′

5′-CGCGCATACTTTGCCACGGACGGCAT-3′
K136A: 5′-CATCCGTGCGCGCATATGCGCG-3′

5′-CGCGCATATGCGCGCACGGATG-3′
R139A: 5′-CAAGTATGCGGCAGAAAAAGGCGTCG-3′

5′-CGACGCCTTTTTCTGCCGCATA-3′
R146A: 5′-GTCGATATTGCGCTTGTCCAAGG-3′

5′-CTTGGACAAGCGCAATATCGACG-3′
K153A: 5′-AAGGAACGGGCGCAAACGGCCGCGTC-CTG-3′

5′-GGACGCGGCCGTTTGCGCCCGTTCC-3′
R156A: 5′-AAAAACGGCGCAGTCCTGAAA-3′

5′-CTTTCAGGACTGCGCCGTTTTTGCCCG-3′
sim4A: 5′-CGTCCGTGGCCGCGTATGCGGCCGAAA-3′

5′-CTTTTTCGGCCGCATACGCGGCCACGGAC-3′

The altered codons are underlined. We also constructed another PSBD mutant, R135A/K136A/R139A/R156A, in which Arg135, Lys136, Arg139, and Arg156 were simultaneously replaced with alanine. To generate this mutant, designated sim4A, plasmid pET11ThDD encoding the R156A mutation, was used as the PCR template. Mutagenesis was carried out by splicing overlap-extension techniques, as described elsewhere (*16, 17*).

Expression of Subgenes and Purification of Proteins. E. coli BL21(DE3) cells transformed with the plasmid pET11-ThDD were grown at 37 °C in LB medium (2 l) supplemented with 50 μg/mL ampicillin, until the A_{600} was between 0.7 and 1.0. The cells were then induced with IPTG (final concentration 1 mM) and incubated for 2 h before being harvested by centrifugation at 6500*g* for 20 min. The pellet was resuspended in 100 mM Tris-HCl buffer, pH 7.5, containing 1 mM EDTA, 0.02% sodium azide, and 0.1 mM PMSF, and the cells were disrupted in a French press at 4 °C under a pressure of 140 MPa. Cell debris were removed by ultracentrifugation at 20000*g* for 30 min and the supernatant was fractionally precipitated by adding solid ammonium sulfate. The fraction precipitating between 30 and 80% saturation was collected by ultracentrifugation at 20000*g* for 30 min and subsequently dissolved in 3 mL of buffer A (20 mM potassium phosphate, pH 7.0, 0.02% sodium azide). Half of the solution (1.5 mL) was loaded onto a Pharmacia Hi-load (16/60) Superdex 200 gel filtration column preequilibrated with buffer A and eluted at a flow rate of 0.5 mL/min. The fractions containing the desired

thrombin-cleavable di-domain (ThDD), as judged by SDS−PAGE, were pooled and subsequently injected onto a Pharmacia Mono Q high-performance anion-exchange column preequilibrated with buffer A. The protein was eluted with buffer B (20 mM potassium phosphate, pH 7.0, 1 M NaCl, 0.02% sodium azide) using a 15−75% gradient over 4 column volumes at a flow rate of 2 mL/min. Fractions containing ThDD were pooled and concentrated by using Centriprep filtration. Recombinant *B. stearothermophilus* E3 was purified as described by Lessard et al. (*18*).

Measurement of CD Spectra. Far-UV CD spectra were recorded by using a Jovin Yvon CD6 spectrometer at room temperature. The sample chamber was constantly flushed with ultrapure nitrogen. The wild-type and mutant ThDDs were dissolved in 20 mM potassium phosphate buffer, pH 7.0, at a final protein concentration of 0.1 mg/mL. CD spectra were recorded from 190 to 245 nm in a 0.1-cm quartz cuvette at 0.1-nm intervals. Six scans for each protein were carried out to obtain an average spectrum.

Lipoylation of the Lipoyl Domain. Lipoylation of the apo-form of the lipoyl domain was conducted in 0.2 mL of 40 mM Tris-HCl, pH 7.5, containing 10 mM ATP, 10 mM MgCl$_2$, 10 mM DL-lipoic acid, 4.0 mg/mL of pure di-domain (ThDD) and 0.05 mg/mL of *E. coli* lipoate protein ligase A (Lp1A). The reaction mixture was incubated for 3 h at 25 °C and complete posttranslational modification of the lipoyl domain was confirmed by electrospray mass spectrometry (*19*). The protein was loaded directly onto a Mono Q high-performance anion-exchange column equilibrated with buffer A and the lipoylated ThDD was eluted by applying a linear gradient (15−75%) of buffer B. Fractions containing the lipoylated ThDD were pooled, desalted and concentrated by Centriprep filtration.

Analysis of Binding Affinity of Mutants. The ability of the mutant ThDDs to bind to E3 was checked by means of nondenaturing PAGE, as described elsewhere (*11*). A ThDD mutant (100 pmol) was incubated with E3 (100 pmol) in 20 mM potassium phosphate buffer, pH 7.0, at room temperature for 5 min and the mixture was then subjected to nondenaturing PAGE (12% acrylamide running gel and 5% acrylamide stacking gel). The interaction of the PSBD with E3 was also investigated by means of SPR detection. The mutant ThDD was immobilized on the CM5 sensor chip using the surface thiol method to react with the lipoyl group on the lipoyl domain, essentially as described by Lessard et al. (*12*). The immobilization level of ThDD mutants was adjusted to be 100−250 response units (RU) to minimize any potential mass transport phenomena. To obtain kinetic parameters, the E3 was injected to interact with the sensor surface for 10 min (association phase) at five different protein concentrations, rising from 25 to 400 nM with gradual 2-fold increments. The flow was then continued for a further 10 min with the first buffer, to obtain the dissociation phase. Experimental data for each mutant were collected from 25 runs (sensorgrams).

Microcalorimetry. Isothermal titration calorimetry (ITC) measurements were carried out in a Microcal calorimeter (MCS-ITC and VP-ITC, Micro Cal, Inc. Northampton, MA) at two different temperatures (25 and 37 °C), as described elsewhere (*13*). The mutant ThDD at a concentration of around 220 μM was injected in 10 μL increments into the reaction cell (cell volume 1.31−1.41 mL) containing E3 at

an approximate concentration of 7.0 μM in the same buffer, until saturation was complete. Concentrations of protein samples were estimated from both amino acid analysis and UV absorbance measurements, assuming A_{280} 0.1% = 1.31 for E3 (dimer M_r = 98 448) and 0.48 for ThDD (M_r = 18 923). Data acquisition and analysis were automatically performed by standard nonlinear regression methods, using the Microcal ORIGIN software package, in terms of a simple binding model. Differential scanning calorimetric (DSC) measurements were also performed as described elsewhere (*13*). The concentrations of samples used for DSC experiments were about 50 μM for ThDD mutants and about 4.0 μM for E3.

Calculation of Accessible Surface Areas. Accessible surface area (ASA) buried upon complex formation was calculated with the program NACCESS (*20*), which utilizes an algorithm created by Lee and Richards (*21*). The crystal structure of the E3-PSBD complex (*8*) and a probe radius of 1.4 Å were the starting points for the calculation. The alanine residue replacing any given residue in the mutant PSBD was modeled with the program SWISS-MODEL (*22*); the PSBD with the modeled alanine residue was used in the surface area calculations. To estimate the change in accessible surface area (ΔASA) during complex formation, the polar and nonpolar surface areas of the free E3 (ASA_{E3}), free PSBD (ASA_{PSBD}) and E3-PSBD complex ($\text{ASA}_{E3+PSBD}$) were calculated for each mutant PSBD studied. The change in either polar or nonpolar accessible surface area was then determined from the equation:

$$\Delta\text{ASA} = \text{ASA}_{E3+PSBD} - (\text{ASA}_{E3} + \text{ASA}_{PSBD})$$

General Protein Chemical Techniques. Nondenaturing PAGE, SDS−PAGE, and amino acid analysis were carried out as described elsewhere (*11, 13*).

RESULTS

Choice of Residues for Replacement. Alanine-scanning mutagenesis was used to dissect the contribution of individual amino acid residues on the surface of the PSBD to the molecular interaction with E3. From the X-ray crystal structure of the E3-PSBD complex (*8*), it is clear that certain positively charged side-chains from PSBD are involved in ionic interactions with negatively charged side-chains from E3. Four basic residues (Arg135, Lys136, Arg139, and Arg156) in PSBD were therefore selected for separate and multiple replacement with alanine. Two uncharged residues (Met131 and Ser133) and two other positively charged residues (Arg146 and Lys153) were also altered, to assess their contribution, if any, to the binding to E3. As shown in Figure 1B, all amino acid residues selected for replacement are located on helix 1 and loop 2 of PSBD and are fully solvent-exposed.

Purification and Characterization of Mutant ThDDs. All the mutant forms of ThDD, generated from subgenes overexpressed in *E. coli* (BL21) cells, were purified to homogeneity as judged by SDS−PAGE (data not shown). As reported elsewhere (*10, 23, 24*), the CD spectrum of ThDD is characteristic of the PSBD, consisting largely of α-helices, plus the LD, composed of two 4-stranded β-sheets. The CD spectra of all the mutant ThDDs showed a strong component characteristic of the α-helices in the PSBD. Few
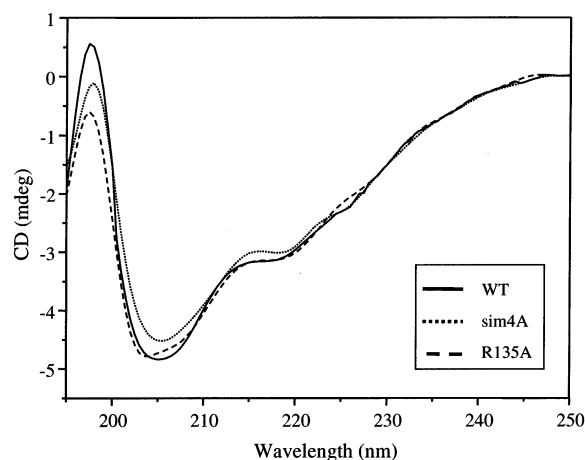
FIGURE 2: Far-UV CD spectra of wild-type and di-domain variants. Solid line, wild type; dashed line, R135A mutant; dotted line, sim4A mutant.
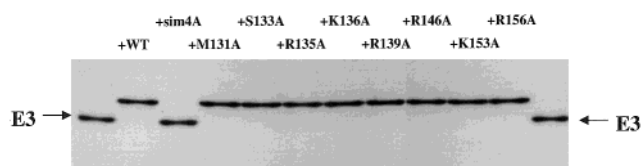
FIGURE 3: Nondenaturing PAGE of wild-type and mutant di-domains (ThDDs) complexed with E3. Pure wild-type and mutant ThDDs (each 100 pmol) were incubated with E3 (100 pmol of dimer) in 20 mM potassium phosphate buffer, pH 7.0 at 20 °C and samples of the mixtures were subjected to nondenaturing PAGE. Retardation of the E3 band is indicative of tight complex formation with the indicated di-domain.

changes, if any, between the spectra of the wild-type and mutant ThDDs were observed, indicating that the overall structure was not significantly distorted by the various amino acid replacements, as expected for the substitution of surface residues (*25*). The CD spectra of two representative mutants (R135A and sim4A) are shown in Figure 2.

Binding of Mutant PSBDs to E3. To investigate the ability of the mutant forms of the PSBD to bind to E3, the mutant ThDDs were each incubated with E3 in 20 mM potassium phosphate buffer, pH 7.0, for 5 min at room temperature and the mixture was then submitted to nondenaturing PAGE (Figure 3). All the single amino acid mutants of ThDD caused the E3 band to be retarded, consistent with tight binding of the PSBD to E3. However, the sim4A (R135A/K136A/R139A/R156A) mutant of ThDD did not retard the E3 band, suggesting that together the four positively charged residues play a major role in the binding to E3, in good agreement with the crystal structure data.

Although nondenaturing PAGE gives an indication of whether the mutant ThDDs can bind tightly to E3, it gives no information about the strength of the interaction. For this, real-time kinetic measurements were required.

Kinetics of Interaction of PSBD Mutants with E3. Real-time rate and equilibrium constants for the interaction of mutant PSBDs with E3 were obtained by SPR detection. One BIAcore sensor chip CM5 contained four flow cells in each of which the lipoylated LD of ThDD could be immobilized. The wild-type ThDD was immobilized in the second flow cell of every sensor chip as an internal reference; the first flow cell was used as a blank. Typical SPR profiles for association of E3 with wild-type and mutant PSBDs,
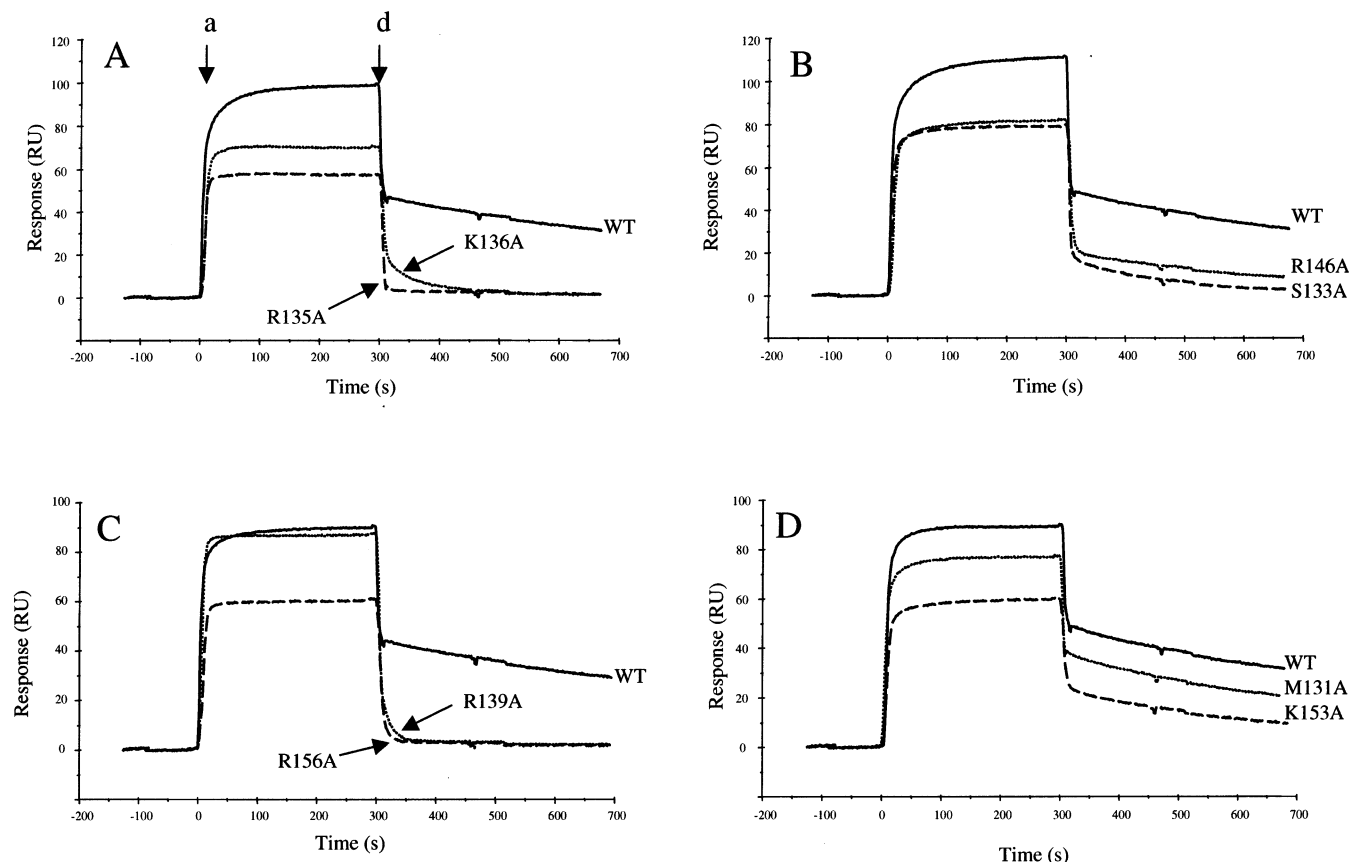
FIGURE 4: SPR sensorgrams (relative response in RU versus time) of wild-type and mutant ThDDs binding to E3. Two different mutants and the wild-type ThDDs were immobilized on the surfaces of three separate flow cells of one CM5 sensor chip. The fourth flow cell was used for a blank sensorgram, in which no protein was immobilized. Wild-type E3 was injected onto the sensor surface using a series of increasing concentrations (25, 50, 100, 200, and 400 nM) and representative sensorgrams (all at 50 nM) are presented in panels A−D. The start of the association and dissociation phases are indicated by the symbols a and d, respectively. Solid line, wild-type ThDD; dashed and dotted lines, mutant ThDDs as indicated.

immobilized by means of the lipoyl group on the LD of the various ThDDs, are presented in Figure 4. As summarized in Table 1, all the kinetic data were obtained as the relative ratio of the SPR response for the immobilized mutant in a given chip to that for the wild-type domain in the same chip. This helped to limit possible experimental variations.

For each sensorgram, values for k_{on}, k_{off}, and K_d (k_{off}/k_{on}) could be determined, the formation and dissociation of the E3-PSBD complex being treated as a pseudo first-order interaction (*12*). For mutants R135A, R139A, and R156A (Figure 4), the association of E3 reached a steady state immediately and subsequently generated rectangular-shaped binding and dissociation curves, which is a good indicator of weakened binding. A large error may be produced by the simultaneous measurement of k_{on} and k_{off} values with the typical fitting method using BIAevaluation software (Pharmacia). Therefore, the equilibrium measurement method (*26*) was used, as follows.

If the pulse of E3 continues long enough for the binding to reach equilibrium, the dissociation equilibrium constant (K_d) can be calculated using the following equation:

$$R_{eq} = R_{max} - K_d R_{eq}/C \qquad (1)$$

where R_{eq} is the amount of bound protein at equilibrium, R_{max} is the maximum protein binding capacity of the surface, and C is the concentration of protein in solution. A Scatchard plot of R_{eq} against R_{eq}/C thus gives the equilibrium dissocia-

Table 1: Relative Ratio of k_{on}, k_{off}, and K_d for Mutant PSBDs Interacting with E3, as Determined by SPR Detection[a]

PSBD	$k_{on}(mut)/$ $k_{on}(wt)$	$k_{off}(mut)/$ $k_{off}(wt)$	$K_d(mut)/$ $K_d(wt)$	$\Delta\Delta G°$ [e]
WT	1.0	1.0	1.0	0
M131A	0.9	1.6	1.8	+0.5
S133A	1.1	4.1	3.7	+0.8
R135A	N.D.	N.D.	120.0[c]	+2.8
K136A	1.0	11.1	11.1[c]	+1.4
R139A	0.8[d]	39.4	49.3[c]	+2.3
R146A	0.9	1.9	2.2	+0.5
K153A	0.8	3.9	4.7	+0.9
R156A	0.9[d]	52.5	58.3[c]	+2.4
sim4A[b]	N.D.[f]	N.D.	N.D.	N.D.

[a] In the case of mutant K136A, fitting method using BIAevaluation software (v3.0) was also employed. No difference between the results of the two methods was observed. The standard errors on kinetic parameters for mutant ThDDs are less than 10%, except for mutant R135A ($\leq$20%). The kinetic parameters of the wild-type PSBD for E3 are $k_{on} = 3.26 \times 10^6$ M^{-1} s^{-1}, $k_{off} = 1.87 \times 10^{-3}$ s^{-1}, $K_d = 5.8 \times 10^{-10}$ M (*12*). [b] Sim4A means simultaneous replacement of residues Arg135, Lys136, Arg139, and Arg156 with alanine. [c] Obtained by equilibrium measurement method or BIAevaluation software (v3.0) (see Materials and Methods). [d] Calculated from k_{off} and K_d. [e] $\Delta\Delta G° = RT$ ln(K_d ratio), where $R = 1.987$ cal/mol K and $T = 298$ K. [f] N. D. = not determined.

tion constant, K_d, from the slope (data not shown) (*27*). The value of R_{eq} was corrected for the contribution of bulk solution to the SPR signal, so the buffer baselines have been

Table 2: Thermodynamic Parameters for Mutant PSBDs Binding to E3[a]

PSBD	$\Delta G°$ [b] (kcal/mol)	$\Delta H°$ [c] (kcal/mol)	$T\Delta S°$ [d] (kcal/mol)	$\Delta S°$ [d] (kcal/molK)
WT	−12.6	+2.2	+14.8	+49.7
M131A	−11.9	+2.2	+14.1	+47.3
R135A	−9.8	−2.6	+7.2	+24.2
K136A	−11.0	+2.8	+13.8	+46.3
R139A	−10.1	+4.7	+14.8	+49.7
R156	−10.2	+5.9	+16.1	+54.0

[a] All the kinetic and thermodynamic parameters are taken from experiments in HBS buffer, pH 7.4, 25 °C. The standard errors on thermodynamic parameters are less than 5%. [b] Calculated from $\Delta G°$ = $RT \ln K_d$, where K_d was obtained from SPR analysis. [c] Measured by ITC experiments. [d] Calculated from $T\Delta S° = \Delta H° − \Delta G°$, where T is 298 K.

subtracted. The k_{off} values were independently determined using the BIAevaluation software and the k_{on} values were then calculated from eq 2:

$$K_d = k_{off}/k_{on} \qquad (2)$$

The kinetic parameters for mutants M131A, S133A, R146A, and K153A were measured using BIAevaluation software, as described elsewhere (*12*). In the case of the mutant K136A, both methods were utilized, and a good agreement between the two K_d values obtained was noted. All experimental results within the range of a reasonable value of chi-square (≤2) were selected.

The R135A mutant of PSBD was found to exhibit a binding affinity 120-fold less than that of wild-type PSBD (Table 1), indicating that this residue is crucial in the formation of the E3-PSBD complex. The R139A and R156A mutations were associated with smaller effects, as was the K136A replacement. Amino acid residues not involved in the ionic interactions (*8*), such as Met131 and Ser133, had little effect on the binding affinity. Two other positively charged surface residues, Arg146 and Lys153, also appeared to make only a very small contribution to binding. In summary, SPR analysis showed that the mutations in the PSBD influenced the dissociation constant (K_d) in the order: R135A ≫ R156A > R139A ≫ K136A > K153A > S133A > R146A > M131A. The fact that the last four residues in this list contributed very little to the interaction is entirely consistent with the crystal structure of the E3-PSBD complex.

Energetics of the Interactions of Mutant PSBDs with E3. Previous ITC experiments (*13*) have demonstrated that the binding of E3 to the wild-type PSBD at 25 °C, pH 7.4, is mainly entropy-driven ($T\Delta S = +14.8$ kcal/mol) and enthalpically unfavorable ($\Delta H = +2.2$ kcal/mol). These thermodynamic parameters were ascribed to the release of bound water molecules from the binding interface as it formed, associated with the salt bridge formation. To identify more precisely the source of these effects, the interaction of the PSBD mutants with E3 was studied by means of ITC at 25 °C, pH 7.4. The four mutants that exhibited $\Delta\Delta G_{binding}$ values of more than +1.0 kcal/mol (Table 2), were chosen for the ITC experiments. The M131A mutant was also included, as a control, since it exhibited the smallest change in dissociation constant (K_d).

The binding free energies ($\Delta G°_{mutant}$) for individual mutant PSBDs were obtained from eq 3

$$\Delta G° = RT \ln K_d \qquad (3)$$

and the $T\Delta S°$ values were calculated from the standard thermodynamic relationship,

$$T\Delta S° = \Delta H° − \Delta G° \qquad (4)$$

where T is the absolute temperature.

In agreement with the SPR analysis, ITC measurements revealed that the R135A mutation had a remarkable effect on the binding of the PSBD to E3. The dissociation constant (K_d) of this mutant was found to be 2.0×10^{-8} M, which was the largest among the various mutants tested. This is, however, about 3.5 times smaller than the K_d value (7.0×10^{-8} M) calculated from the results of SPR detection (Table 1). Given the technical differences between the two methods (e.g., one employs an immobilization procedure and the other does not), this disagreement is modest. At 25 °C, the binding of the R135A mutant of PSBD to E3 was characterized by a small but negative enthalpy ($\Delta H° = −2.6$ kcal/mol) and a less positive entropy change ($T\Delta S° = +7.2$ kcal/mol).

The other mutations to the PSBD caused no significant change in the entropic contribution to binding (Table 2). The R139A and R156A mutations, in particular, gave rise to an enthalpy change yet more unfavorable than that measured for the wild-type interaction, but generated little change in $T\Delta S$. According to the E3-PSBD crystal structure, Arg139 is fully solvent-exposed, whereas Arg156 is completely buried in the interface. There is thus no obvious explanation for the similarity of the effects of these mutations on the thermodynamic parameters. It is, however, clear that residues Arg139 and Arg156 can be excluded as a source of the favorable entropy change in the interaction between E3 and wild-type PSBD, although their mutation causes a major loss of binding affinity.

Changes in Heat Capacity. In general, hydrophobic interactions are inclined to generate negative contributions to the heat capacity of binding, whereas electrostatic interactions are associated with positive changes (*28−30*). It has been suggested, therefore, that mutations that weaken the hydrophobic contribution to folding or association should make ΔC_p less negative (positive $\Delta\Delta C_p$), whereas weakened polar interactions should make ΔC_p more negative (a negative $\Delta\Delta C_p$) (*31*). To estimate the heat capacity changes in binding the mutant PSBDs, the ITC experiments were repeated at a temperature of 37 °C. The variation in enthalpy with respect to temperature is summarized in Table 3. These quantities were plotted over a range of temperature (data not shown) to calculate the heat capacity change from the relationship:

$$\Delta C_p = \delta(\Delta H)/\delta T \qquad (5)$$

As shown in Table 3, all the mutant PSBDs that were tested generated a negative $\Delta\Delta C_p$. This was expected, owing to the removal of charged residues at the mutated site. The R135A mutant occasioned the largest decrease in ΔC_p. According to the buried accessible surface area calculations (*20*), the R135A mutation should cause a large loss of buried polar area ($\Delta\Delta A_{polar} = 81.1$ Å²), while leaving the apolar

Table 3: Enthalpy and Heat Capacity Changes on Binding of E3 to Mutant PSBDs[a]

	(kcal/mol)		(kcal/molK)		(kcal/molK)		(Å²)	
PSBD	$\Delta H^{25\,°C}$	$\Delta H^{37\,°C}$	$\Delta C_p{}^b$	$\Delta\Delta C_p{}^c$	$\Delta C_p{}^d$	$\Delta\Delta C_p{}^c$	ΔA_{polar}	ΔA_{apolar}
WT	+2.2	−1.8	−316[e]	0	−187	0	449.2	674.9
M131A	+2.2	−1.9	−342	−26	−162	25	445.6	617.6
R135A	−2.6	−8.4	−483	−167	−210	−23	368.1	678.2
K136A	+2.8	−2.5	−442	−126	−182	5	395.9	632.7
R139A	+4.7	0.0	−392	−76	−204	−17	391.3	614.7
R156A	+5.9	+1.	−383	−67	−199	−12	422.2	685.8

[a] The standard errors on thermodynamic parameters are less than 5%. [b] Calculated from the slope of the regression line of the linear fit of the enthalpies measured at two different temperatures (25 and 37 °C). [c] Difference in ΔC_p relative to E3-wild-type PSBD complex. [d] Calculated from the equation relating the polar (ΔA_{polar}) and nonpolar (ΔA_{apolar}) surface areas buried upon interaction. [e] Taken from previous results (13).

Table 4: Midpoint Melting Temperatures of E3 Complexed with Mutant PSBDs

protein	$T_m{}^a$ (°C)
E3 alone	91.0
E3 + wild-type PSBD	97.0
E3 + M131A mutant	97.0
E3 + R135A mutant	92.0
E3 + K136A mutant	94.2
E3 + R139A mutant	93.0
E3 + R156A mutant	93.5

[a] Obtained from DSC measurements. The standard errors are less than 5%.

buried area unchanged (Table 3). This loss of buried polar area results mainly from the difference in solvent-accessible polar area between the wild-type PSBD (722.9 Å²) and mutant R135A (646.6 Å²) since there is little difference between the E3-PSBD (10390.7 Å²) and E3-R135A (10395.5 Å²) complexes (see Materials and Methods for the buried surface area calculation). These results point to the polar group of Arg135 as being highly solvent-exposed in the free domain, but fully buried in the complex and playing a leading part in making the salt bridge with E3 in the contact area. The negative $\Delta\Delta C_p$ value for the R135A mutant observed here agrees well with a decrease in burial of polar groups in the interface.

The Effect of Mutant PSBDs on the Thermal Stability of E3. The thermal stabilities of E3-PSBD mutants were investigated by DSC experiments (data not shown). The thermal stability of the E3 dimer (T_m = 91 °C) was improved by complex formation with the wild-type PSBD (T_m = 97 °C), as indicated in Table 4. The R135A mutant showed the smallest increase in T_m value (to 92 °C). Arg135 evidently plays an important part in conferring thermal stability on the complex. The other mutants in which charged residues were replaced with alanine also exhibited significant effects on the ability to confer extra thermal stability on the complex with E3. In contrast, the mutant M131A, which showed little effect on the binding affinity and thermodynamic parameters, did not change the value of T_m.

DISCUSSION

The changes in the K_d values of the mutant PSBD-E3 complexes are all due mainly to changes in the rate of dissociation (k_{off}). It has been observed elsewhere that the value of k_{off} is dependent on specific short-range interactions (van der Waals interactions, hydrogen bonds, hydrophobic interactions, and salt bridges) between proteins but rarely affected by the diffusion rate at which the two separated

proteins move away from each other (32). The residues in PSBD whose replacement with Ala had the biggest effect on K_d (i.e., Arg135, Lys136, Arg139, and Arg156) are implicated in short-range interactions with E3 in the crystal structure of the E3-PSBD complex (8). Thus, the SPR results are fully consistent with the structural data, and enable us to point to Arg135 as being of particular importance, with Arg139 and Arg156 also making significant contributions to the binding of E3 (Table 1).

According to the structural information, Arg135 and Arg139 of the E2 PSBD form an electrostatic "zipper" with Asp344 and Glu431 of E3 monomer B at the binding interface (Figure 1C). This tight conformation facilitates the exclusion of water molecules from the binding interface and/ or alters the structure of water in the vicinity of the salt bridges formed. In an homology model of the E3-R135A mutant complex (Figure 1D), the replacement of the guanidium side-chain of Arg135 with a methyl group creates a cavity (approximate volume 92 Å³) in the binding interface, which is surrounded by the Oδ2 atom of the side-chain of Asp344, the Oε2 atom of the side-chain of Glu431 and the O atom of the backbone at both residues provided by E3 monomer B. This cavity could allow room for water molecules to form hydrogen bonds with the acidic side-chains of Asp344 and Glu431, thereby generating the more favorable enthalpy change and the smaller but still favorable entropy change. Recent studies on the structural response to mutation at the interface of the barnase−barstar complex (33) suggest that water molecules can fill the binding pocket and cavities created by mutation. These water molecules were also found to mimic the deleted side-chains by occupying positions close to the non-carbon atoms of truncated side-chains and remaking many hydrogen bonds. The structural response of water molecules to cavity-creating mutations at protein−protein interfaces has been reported elsewhere: for instance, lysozyme-antibody interactions (34, 35) and influenza virus N9 neuraminidase−antibody interactions (36).

Previous work (13) has demonstrated a lack of correlation between the experimentally measured and calculated ΔC_p values for the E3-wild-type PSBD interaction. All the ΔC_p values calculated from the equations of Murphy and Freire (37) and Spolar and Record (38) were less negative than those experimentally determined ΔC_p values. These significant discrepancies (summarized in Table 3) show that the equations used (37, 38) are inadequate in predicting ΔC_p values from the surface area buried in the E3-PSBD interaction.

The reductions in the T_m values of the complexes formed between E3 and mutant PSBDs, compared with the wild-

type E3-PSBD complex (Table 4), varied in the same way as the effect of the mutations on the K_d values (Table 1). Thus, the R135A mutation caused the biggest change in K_d and the smallest increase in T_m, and vice versa for the M131A mutation. All the experiments reported above are consistent with the importance of ionic interactions in promoting the association of E3 with the PSBD of E2 and of the buried salt bridges in conferring stability on the complex. Not all the residues involved contribute equally: Arg135 in the PSBD is evidently of particular importance in the tightness of the binding and, although it is not a hydrophobic interaction, as a major source of the large positive entropy change that accompanies complex formation.

ACKNOWLEDGMENT

REFERENCES

1. Reed, L. J., and Hackert, M. L. (1990) *J. Biol. Chem. 265*, 8971−8974.
2. Perham, R. N. (1991) *Biochemistry 30*, 8501−8512.
3. de Kok, A., Hengeveld, A. F., Martin, A., and Westphal, A. H. (1998) *Biochim. Biophys. Acta 1385*, 353−366.
4. Perham, R. N. (2000) *Annu. Rev. Biochem. 69*, 961−1004.
5. Hawkins, C. F., Borges, A., and Perham, R. N. (1990) *Eur. J. Biochem. 191*, 337−346.
6. Izard, T., Ævarsson, A., Allen, M. D., Westphal, A. H., Perham, R. N., de Kok, A., and Hol, W. G. J. (1999) *Proc. Natl. Acad. Sci. U.S.A. 96*, 1240−1245.
7. Kalia, Y. N., Brocklehurst, S. M., Hipps, D. S., Appella, E., Sakaguchi, K., and Perham, R. N. (1993) *J. Mol. Biol. 230*, 323−341.
8. Mande, S. S., Sarfaty, S., Allen, M. D., Perham, R. N., and Hol, W. G. J. (1996) *Structure 4*, 277−286.
9. Packman, L. C., Borges, A., and Perham, R. N. (1988) *Biochem. J. 252*, 79−86.
10. Hipps, D. S., Packman, L. C., Allen, M. D., Fuller, C., Sakaguchi, K., Appella, E., and Perham, R. N. (1994) *Biochem. J. 297*, 137−143.
11. Lessard, I. A. D., and Perham, R. N. (1995) *Biochem. J. 306*, 727−733.
12. Lessard, I. A. D., Fuller, C., and Perham, R. N. (1996) *Biochemistry 35*, 16863−16870.
13. Jung, H. I., Bowden, S. J., Cooper, A., and Perham, R. N. (2002) *Protein Sci. 11*, 1091−1100.
14. Allen, M. D. (1995) Ph.D. Thesis, Department of Biochemistry, University of Cambridge, UK.
15. Morris, T. W., Reed, K. E., and Cronan, J. E., Jr., (1994) *J. Biol. Chem. 269*, 16091−16100.
16. Ho, S. N., Hunt, H. D., Horton, R. M., Pullen, J. K., and Pease, L. R. (1989) *Gene 77*, 51−59.
17. Horton, R. M., Hunt, H. D., Ho, S. N., Pullen, J. K., and Pease, L. R. (1989) *Gene 77*, 61−68.
18. Lessard, I. A. D., Domingo, G. J., Borges, A and Perham, R N. (1998) *Eur. J. Biochem. 258*, 491−501.
19. Jones, D. D., Horne, H. J., Reche, P. A., and Perham, R. N. (2000) *J. Mol. Biol. 295*, 289−306.
20. Hubbard, S. J., and Thornton, J. M. (1993) NACCESS, Computer Program, Department of Biochemistry and Molecular Biology, University College London. Further information can be found at http://sjh.bi.umist.ac.uk/naccess.html.
21. Lee, B. K., and Richards, F. M. (1971) *J. Mol. Biol. 55*, 379−400.
22. Guex, N., and Peitsch, M. C. (1997) *Electrophoresis 18*, 2714−2723.
23. Wallis, N. G., Allen, M. D., Broadhurst, R. W., Lessard, I. A. D., and Perham, R. N. (1996) *J. Mol. Biol. 263*, 463−474.
24. Spector, S., Kuhlman, B., Fairman, R., Wong, E., Boice, J. A., and Raleigh, D. P. (1998) *J. Mol. Biol. 276*, 476−489.
25. Bowie, J. U., Reidhaar-Olsen, J. F., Lim, W. A., and Sauer, R. T. (1990) *Science 247*, 1306−1310.
26. Pharmacia Biosensor AB, Application note 301.
27. Karlsson, R., Michaelsson, A., and Mattsson, L. (1991) *J. Immunol. Methods, 145*, 229−240.
28. Sturtevant, J. M. (1977) *Proc. Natl. Acad. Sci. U.S.A. 74*, 2236−2240.
29. Makhataolze, G. I., and Privalov, P. L. (1990) *J. Mol. Biol. 213*, 375−384.
30. Livingstone, J. R., Spolar, R. S., and Record, M. T. (1991) *Biochemistry 30*, 4237−4244.
31. Kelly, R. F., and O'Connell, M. P. (1993) *Biochemistry 32*, 6828−6835.
32. Selzer, T., Albeck, S., and Schreiber, G. (2000) *Nat. Struct. Biol. 7*, 537−541.
33. Vaughan, C. K., Buckle, A. M., and Fersht, A. R. (1999) *J. Mol. Biol. 286*, 1487−1506.
34. Chacko, S., Silverton, E., Kam-Morgan, L., Smith-Gill, S., Cohen, G., and Davies, D. (1995) *J. Mol. Biol. 245*, 261−274.
35. Ysern, X., Fields, B. A., Bhat, T. N., Goldbaum, F. A., Dall'Acqua, W., Schwarz, F. P., Poljak, R. J., and Mariuzza, R. A. (1994) *J. Mol. Biol. 238*, 496−500.
36. Tulip, W. R., Varghese, J. N., Webster, R. G., Laver, W. G., and Colman, P. M. (1992) *J. Mol. Biol. 227*, 149−159.
37. Murphy, K. P., and Freire, E. (1992) *Adv. Protein Chem. 43*, 313−361.
38. Spolar, R. S., and Record, M. T. (1994) *Science 263*, 777−784.
39. Kraulis, P. (1991) *J. Appl. Crystallog. 24*, 946−950.